INTERNATIONAL JOURNAL OF REFRIGERATION 75 (2017) 239–249

Available online at www.sciencedirect.com

ScienceDirect

journal homepage: www.elsevier.com/locate/ijrefrig

Effects of the driving voltage waveform on the performance of the Stirling-type pulse tube cryocooler driven by the moving-coil linear compressor

Jun Tan [a,b], *Haizheng Dang* [a,*]

[a] *National Laboratory for Infrared Physics, Shanghai Institute of Technical Physics, Chinese Academy of Sciences, 500 Yutian Road, Shanghai 200083, China*

[b] *University of Chinese Academy of Sciences, No. 19A Yuquan Road, Beijing 100049, China*

ARTICLE INFO

Article history:
Received 28 June 2016
Received in revised form 6 December 2016
Accepted 25 December 2016
Available online 28 December 2016

Keywords:
Driving voltage waveform
Moving-coil linear compressor
Stirling-type pulse tube cryocooler
Compressor motor efficiency
Cooling performance

ABSTRACT

The effects of three typical waveforms, namely, sine, trapezoid and smeared sine, on the performance of the Stirling-type pulse tube cryocooler (SPTC) driven by the moving-coil linear compressor are analyzed and studied experimentally. The results indicate that the dynamic pressure at the inlet of the cold finger has a weak relation with the driving voltage waveform, but the latter plays an important role in affecting both the motor efficiency and the SPTC cooling performance. In the tested range, either the cooling efficiency or the motor efficiency under the smeared sine waveform is the highest, while that under the sine waveform is the lowest. Moreover, given that the input power is below 30 W, the motor efficiencies under both smeared sine and trapezoid waveforms exceed 90%, which suggests a promising approach to achieve a linear compressor with a very high motor efficiency by optimizing the voltage waveform.

Influence de la forme d'onde de la tension de commande sur la performance d'un cryorefroidisseur à tube à pulsation de type Stirling alimenté par le compresseur linéaire à serpentin mobile

Mots clés : Forme d'onde de la tension de commande ; Compresseur linéaire à serpentin mobile ; Cryorefroidisseur à tube à pulsation de type Stirling ; Rendement du moteur de compresseur ; Performance de refroidissement

* *Corresponding author.* National Laboratory for Infrared Physics, Shanghai Institute of Technical Physics, Chinese Academy of Sciences, 500 Yutian Road, Shanghai 200083, China. Fax: +86 21 65830734.
E-mail address: haizheng.dang@mail.sitp.ac.cn (H. Dang).

http://dx.doi.org/10.1016/j.ijrefrig.2016.12.017

Nomenclature

A_p	cross sectional area of piston
b	mechanical damp
B	magnitude of magnetic field
i	current
I_{rms}	root mean square of the current
k_x	axial stiffness of flexure springs
L	coil length
L_e	coil inductance
m	moving mass
p	dynamic pressure in compression space
p_b	dynamic pressure on backside of piston
Q	Joule heat of motor coil
R_e	coil resistance
t	time
u	voltage
W_e	electric input power
x	displacement of the piston
η_{motor}	motor efficiency

1. Introduction

The pulse tube cryocooler (PTC), first proposed in the early 1960s (Gifford and Longsworth, 1965), has achieved significant progress in the past five decades (Ross, 2007). Without any moving component at the cold end, the wear-out in the cold finger is eliminated and both the vibration and the electromagnetic interference at the cold end are substantially reduced compared with the conventional regenerative cryocoolers. Based on the driver used, the commonly-used PTCs can be further divided into the GM-type PTC and the Stirling-type PTC (SPTC). The SPTC is driven by the linear compressor, which minimizes the wear-out between the piston and the cylinder by eliminating the radial forces exerted on the piston, and thus the SPTC is endowed with some intrinsic merits such as compactness, light weight, low vibration and EMI, high reliability and long operation lifetime, which have a strong appeal to many special fields, especially in space (Dang, 2015; Ross, 2007).

For many practical applications, especially in the special aerospace environment where the power supply is relatively limited and the rejection condition is extremely adverse, the high thermodynamic efficiencies of the SPTCs are often emphasized (Dang et al., 2016). A wide variety of theoretical and experimental investigations have been carried out to improve the efficiency of the SPTC (Dang, 2012; Dang et al., 2016; Ki and Jeong, 2012; Ross, 2007; Walker and Bingham, 1994), which mainly include the improvements of the geometrical parameters such as dimensions, arrangements and geometrical structures, and the optimizations on the operating parameters as well. The operating parameters play a key role in understanding the working mechanisms of both the SPTC and its compressor, and also in enhancing both the compressor motor efficiency and the cooler performance. However, the performed optimizations on them mainly focus on the frequency, charge pressure, hot heat exchanger temperature, phase-shifting, and input voltage or current, etc., whereas another important parameter, namely, the driving voltage waveform, is often overlooked.

In the cryogenic field, the moving-coil linear compressor has already become the main driver of the long-life SPTCs due to the proven high efficiency and reliability for about three decades (Davey, 1990; Marquardt et al., 1993; Bailey et al., 2001; Ross, 2007; Dang, 2015), which are attributed to the sustained studies of the linear compressor and its dynamic and thermodynamic characteristics to a great extent (Davey, 1990; Marquardt et al., 1993; Kim et al., 2009; Bailey et al., 2010–2011; Bradshaw et al., 2011, 2013; Ki and Jeong, 2012; Liang et al., 2014; Dang et al., 2016). However, few attempts have been made in adjusting driving voltage waveform of the linear compressor to achieve the higher compressor motor efficiency or the better cooler performance. In practice, the driving voltage waveform of the linear compressor can influence a SPTC from two aspects. On the one hand, the driving voltage waveform itself can directly affect the motor current which will influence the motor efficiency. On the other hand, the waveform can also indirectly influence the cooling efficiency of the PTC cold finger, in which an obvious difference can be found between the usually-used trapezoidal waveform for G-M type PTC and the commonly-used sine waveform for SPTC. The working mechanism of the SPTC can be analogized as a similar regenerative thermodynamic cycle to that of the Stirling cooler, in which the displacer of the Stirling cryocooler is replaced by the pulse tube and phase shifters (Kittel et al., 1996). As well-known, the Stirling cycle consists of four processes, namely, two isochoric ones and two isothermal ones, which are realized by the movements of the compressor piston and displacer piston, in which the driving voltage plays a leading role in controlling the movements of both pistons. For a SPTC without the actual displacer piston, the thermodynamic processes are dominated by the only piston of the linear compressor. Therefore, compared with the Stirling cryocooler, the driving voltage will have much more important and complicated effects on the motor performance of the linear compressor and subsequently on the cooling performance of the SPTC as a whole.

In view of the significant effects of the driving voltage waveform, in this paper, two kinds of optimized driving voltage waveforms will be proposed, namely, trapezoid and sinusoidal-like with the crest and trough horizontal (smeared sine) so as to compare with the commonly-used sine waveform, and then the corresponding theoretical and experimental investigations and comparisons will be made to achieve an in-depth understanding of their specific influences on the SPTC performance discussed above.

2. Theoretical analyses and waveform modulations

Fig. 1 shows the schematic of a typical moving-coil linear compressor. The dual-opposed configuration is used to reduce the compressor vibration. Each half comprises a pressure vessel, a cylinder, two sets of flexure springs, a piston, and a linear motor composed of a permanent magnet, moving coils and two return irons, in which the piston, the coils and the flexure springs will oscillate during operation, and the clearance seal

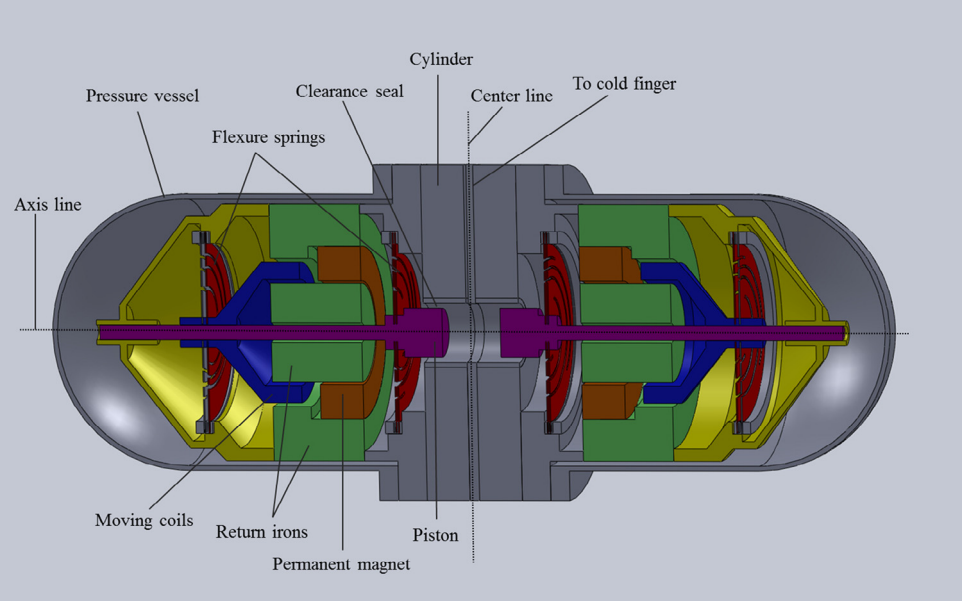

Fig. 1 – A schematic of the dual-opposed moving-coil linear compressor.

acts as the dynamic seal between the piston and the cylinder, thereby eliminating the source of rubbing wear and the necessity of oil lubrication.

As well known, in a Stirling cryocooler, the ideal movements of both compressor piston and displacer piston are shown in Fig. 2, which are all discontinuous (Walker and Bingham, 1994). However, in practice, a driving source to provide such movements is very difficult to get. The AC power supply is one of the most common driving sources to provide periodical drive, and thus is used to acquire the approximately ideal movements for the Stirling cryocooler. In the same way, in a SPTC, the similar AC power is also employed and thus cannot provide the ideal movements of the compressor pistons, either. The deviation from the ideal movements would lead to the deterioration of the SPTC performance. But it should be pointed out that, with the rapid development of the driving electronics, the control of the driver becomes easier and it is feasible to obtain a variety of types of voltage waveform.

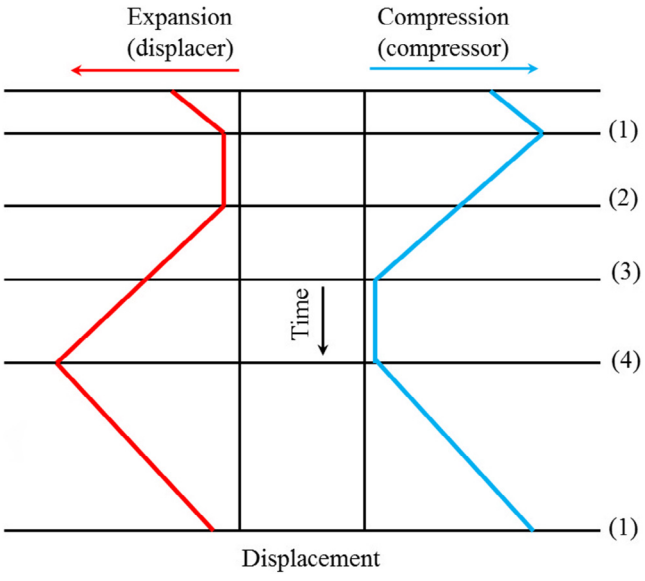

Fig. 2 – Ideal movements of the pistons in the Stirling cryocooler.

For the motor of a moving-coil linear compressor, according to the balances of both electric potential and force, relations between the current, voltage, and piston displacement can be written as (Kim et al., 2009; Marquardt et al., 1993):

$$u(t) = L_e \frac{di(t)}{dt} + R_e i(t) + BL \frac{dx}{dt} \tag{1}$$

$$LBi(t) = m \frac{d^2x(t)}{dt} + b \frac{dx(t)}{dt} + k_x x(t) + (p(t) - p_B(t)) A_p \tag{2}$$

where $u(t)$, $i(t)$ and $x(t)$ are the voltage, current and piston displacement, $p(t)$ and $p_B(t)$ are the dynamic pressure in the compression space and on the backside of the piston respectively, L_e, R_e and L are the inductance, resistance and wire length of the coil, t is the time and B is the magnitude of magnetic field, m is the moving mass, b is the mechanical damp, k_x is the axial stiffness of flexure springs, and A_p is the cross-sectional area of the piston.

Fig. 3 illustrates the relation between the current and other terms. According to Eq. (2), the displacement waveform exerts a direct effect on the values of displacement terms, especially on its first order and second order derivative terms. Hence, the motor current will vary with it accordingly. Moreover, the main motor losses are the joule loss which is in proportion to the square of the current. Hence, the motor efficiency is significantly affected by the displacement waveform.

Compared with the displacement, the driving voltage can be adjusted much more easily. Combining Eqs. (1) and (2), the relation between the voltage and the piston displacement can be achieved as follows:

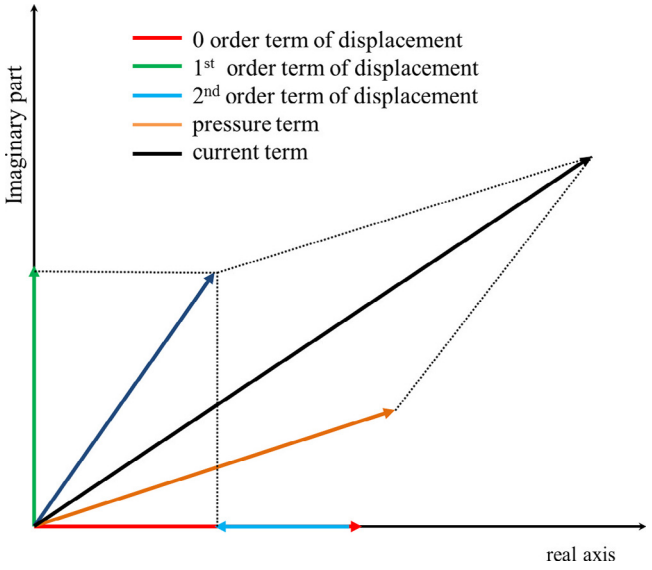

Fig. 3 – Relations between the terms of displacement and current term.

$$u(t)=\frac{k_x R_e}{BL}x(t)+\left(\frac{k_x L_e}{BL}+\frac{bR_e}{BL}+BL\right)\frac{dx(t)}{dt}+\left(\frac{mR_e}{BL}+\frac{bL_e}{BL}\right)\frac{d^2x(t)}{dt}+\frac{mL_e}{BL}\frac{d^3x(t)}{dt}+\frac{R_e A_p}{BL}(p(t)-p_B(t)) \quad (3)$$

The voltage is linked to the third order, the second order, the first order and the zeroth order derivative terms of the piston displacement. According to Eq. (3), the piston movement can be designed through the drive voltage waveform. In this paper, two types of driving voltage waveform are proposed, trapezoid waveform and a waveform named here as smeared sine. Then they will be analyzed and compared with the sine waveform. Their wave shapes are shown in Fig. 4.

With the sinusoidal piston displacement, the third order, the second order, and the first order derivative terms of the piston displacement all vary sinusoidally, and the pressure terms in Eq. (3) can also be regarded as the sine waveform. Moreover, each term on the right side of Eq. (3) has the same angular frequency. After combining the similar terms, it is found that the terms on the right side of Eq. (3) can be simplified as one sinusoidal term with the previous angular frequency, which means the driving voltage and the piston displacement have the same frequency, but different phase angles. Therefore, AC power can be directly used to modulate the voltage for the compressor piston to obtain the sinusoidal displacement.

The way to get the trapezoid waveform piston displacement is similar. Three variation tendencies exist in the trapezoid waveform, in which one increases linearly, one remains constant and another decreases linearly. According to Eq. (3), the needed voltage can be obtained by the combination of the above different cases. For both the linear increase and the linear decrease parts, both the third order and the second order derivative terms of the piston displacement are zero, while the first order one remains constant. For the constant part, the third order, the second order and the first order derivative terms are all equal to zero. In view of that the dynamic pressures all vary with the same tendency as that of the piston, after mathematical processes it is found that the voltage to modulate the trapezoid piston displacement can be roughly considered as the trapezoid waveform with a phase difference.

The smeared sine waveform shown in Fig. 4 combines the characteristics of both sine and trapezoid waveforms. What it differs from the sine waveform is that both crest and trough of the waveform are constant. Based on Eq. (3), the needed voltage to gain the piston displacement of the smeared sine waveform approximates to the smeared sine waveform with a phase difference.

For a SPTC, the cooling performance is affected by the phase relation between the dynamic pressure and the volume flow rate. The phase relations under the sine waveform and the smeared sine waveform at the inlet of the cold finger are compared in Fig. 5. For an optimized cold finger under the sine waveform, the volume flow rate should lead the pressure by φ, while for the smeared sine waveform, the constant part at the crest and trough will cause the volume flow rate to lag by some degrees relative to that of the sine waveform. The new phase difference φ' is smaller than φ, and thus the cooling performance is affected. Therefore, the voltage waveform also has a significant impact on the cooling performance of the cold finger.

To achieve both trapezoid and smeared sine waveforms, the pulse width modulation (PWM) technique is employed and the

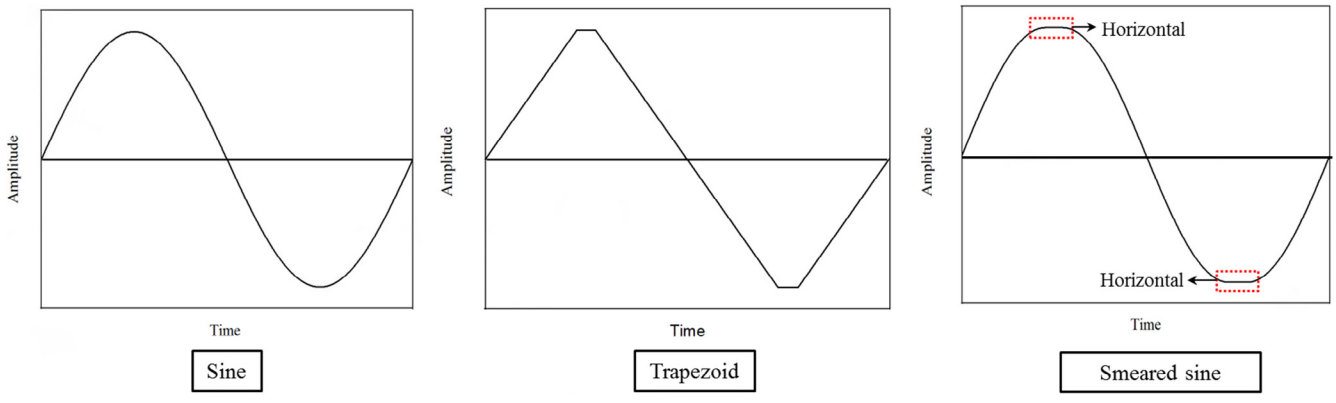

Fig. 4 – Three types of voltage waveforms: sine, trapezoid and smeared sine.

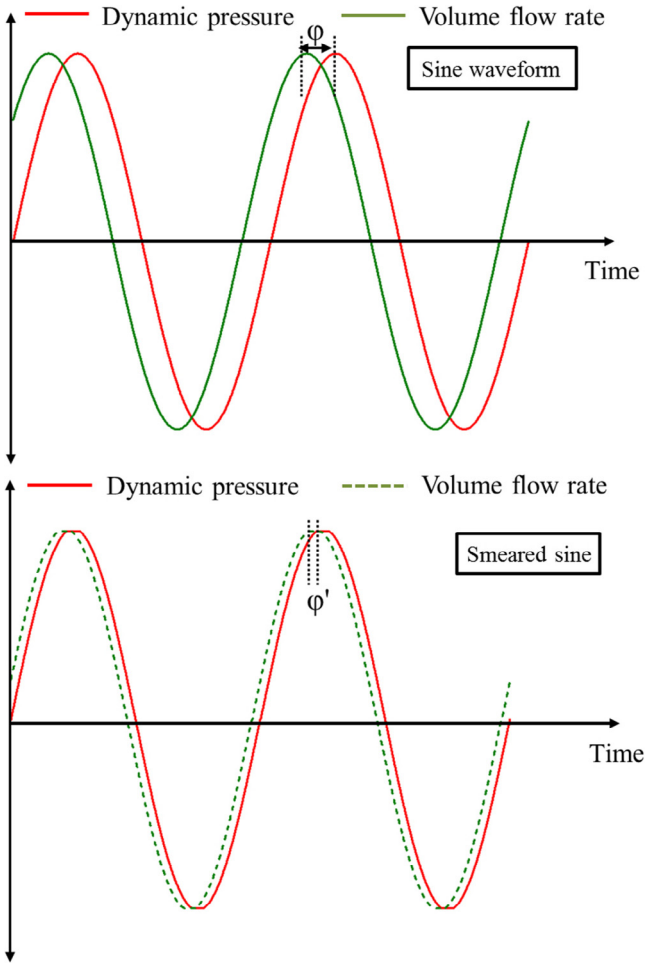

Fig. 5 – Effects of voltage waveform on the phase relation between pressure and volume flow rate.

corresponding electronics of the voltage waveform generator are developed, in which the key point is to achieve a periodical waveform modulated by the pulse wave of high frequency (Flaxer, 2003; Willems et al., 2009). The modulated waveform is divided into many small parts, and the average value of each part can be designed by the adjustment of the duty cycle during each pulse wave period. For example, Fig. 6 shows the modulation of trapezoid waveform through PWM. At first, the duty cycle of the pulse wave is 50% at the equilibrium position and decreases linearly to 0% at the trough, retains 0% for the constant part, and then increases linearly to 100% at the crest, remains 100% for the constant part, finally decreases linearly to 50% at the equilibrium position and finishes the modulation of one period of the trapezoid waveform. The voltage of the smeared sine waveform can also be modulated similarly.

3. Experimental performance characteristic

To make comparisons of both compressor motor efficiency and cooling performance of the SPTC under the three types of driving voltage waveforms, the dedicated experiments have been conducted on a coaxial SPTC driven by a dual-opposed moving-coil linear compressor, both developed in the authors' laboratory. The specific geometric dimensions of the SPTC along with its dual-opposed linear compressor are given in Tables 1 and 2, respectively.

Figs. 7 and 8 show the schematic and the photograph of the experimental setup, respectively. The pulse tube cold finger to be tested is sealed in a Dewar. The signal generator electronics provides the needed voltage waveforms to the H bridge power amplifier electronics to control the drive voltage waveform of the linear compressor and a power meter is used to monitor and measure the input power, input voltage and input

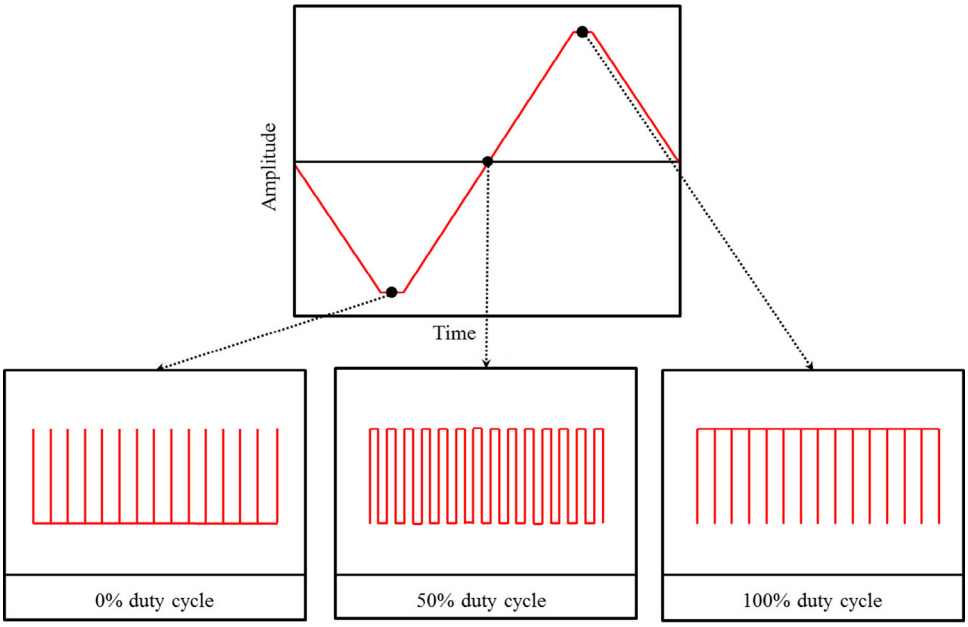

Fig. 6 – Modulation of the trapezoid waveform through PWM.

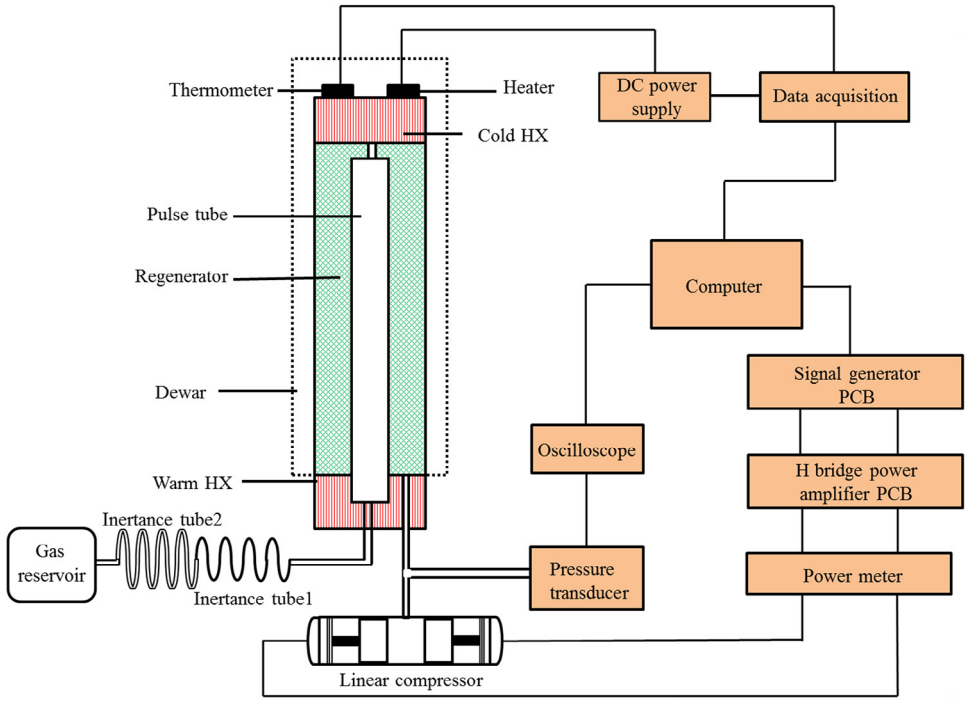

Fig. 7 – A schematic of the experimental setup.

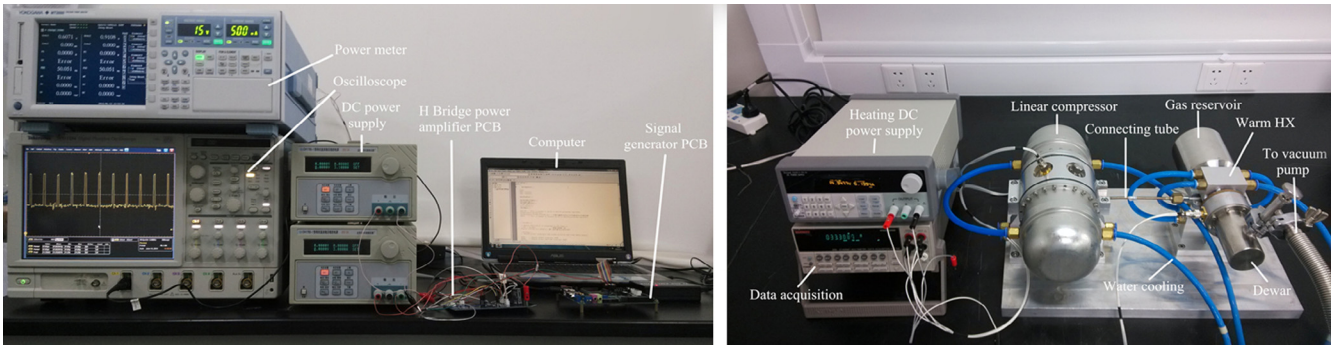

Fig. 8 – Photographs of the experimental setup.

Table 1 – Parameters of each motor of the dual-opposed linear compressor.

Parameters	Values
Magnitude of magnetic field (B)	1.11 T
Coil length (L)	15 m
Coil resistance(R_e)	3.0 Ω
Moving mass (m)	200 g
Flexure spring stiffness (k_x)	4500 N/m
Mechanical damp (b)	4.5 N·s/m
Piston diameter (D_p)	20 mm

Table 2 – Parameters of the components of the cold finger.

Parameters	Values
Connecting tube length	150 mm
Connecting tube diameter	4 mm
Regenerator length	63 mm
Regenerator diameter	28.7 mm
Pulse tube length	95 mm
Pulse tube diameter	13 mm
Inertance tube 1 length	2250 mm
Inertance tube 1 diameter	3.7 mm
Inertance tube 2 length	4100 mm
Inertance tube 2 diameter	7.6 mm
Gas reservoir	400 cm^3

Table 3 – Dynamic pressure under different input powers and voltage waveforms.

Input power (W)	Dynamic pressure (peak to peak/MPa)		
	Sine	Trapezoid	Smeared sine
5	0.1200	0.1165	0.1145
10	0.1495	0.1511	0.1505
20	0.1792	0.1813	0.1800
30	0.1971	0.1963	0.1965
40	0.2120	0.2115	0.2125
50	0.2249	–	0.2255

current. A pressure transducer is installed at the outlet of the linear compressor and the dynamic pressure is measured through the oscilloscope. A data acquisition connected to both the temperature sensor and heater is used to monitor the temperature of the cold head and cooling capacity as well.

Based on the previous test results, the optimal operating frequency of 48 Hz under the sine waveform is chosen as the tested frequency and the charge pressure is 3.3 MPa with helium as the working fluid. The reject temperature is fixed at 300 K. The experimental results of the relations between the peak to peak value of the dynamic pressure and the input power under three types of voltage waveform are given in Table 3. In an input power ranging from 5 W to 50 W, the dynamic pressures under three types of voltage waveform are very close, with the largest deviation being below 4.6%, which indicates that the dynamic pressure is a weak function of these voltage waveforms. Furthermore, Fig. 9 shows the experimental results of the dynamic pressure under the three types of driving voltage waveform. It is observed that, generally speaking, for the three different voltage waveforms, the wave shapes of the dynamic pressure are all sine-like without the evident difference. However, compared with the smooth dynamic pressure wave shape under the sine waveform, there exist some burrs in those under both the smeared sine waveform voltage and the trapezoid waveform voltage, which are caused by the discontinuity of the driving voltage. Therefore, according to the experimental results in Table 3 and Fig. 9, a conclusion can be arrived at that the driving voltage waveform will have slight effects on the dynamic pressure of the cold finger from two aspects, one is on its amplitude and the other on its wave shape.

The comparisons of the cooler performances under the three types of driving voltage waveforms are shown in Fig. 10. For the sine waveform, with the cooling capacity changing from 0.2 W to 2.5 W, the corresponding input power increases from 41.2 W to 69 W. In the case of the trapezoid waveform, the discontinuity of the voltage waveform introduces unacceptable compressor vibration when the electric input power is larger than 43 W, so only two test points, 0.2 W and 0.5 W at 80 K can be achieved, with the input powers of 38.6 W and 42.8 W, respectively. And in the case of smeared sine waveform, the similar compressor vibration occurs once the input power is larger than 60 W. With the cooling capacity varying from 0.2 W to 2 W, the corresponding input power increases from 37.6 W to 59.5 W. In the test range, the SPTC under both the trapezoid and the smeared sine waveforms show better cooling performance than that of the sine waveform, which verifies the above-mentioned analyses that the waveform of driving

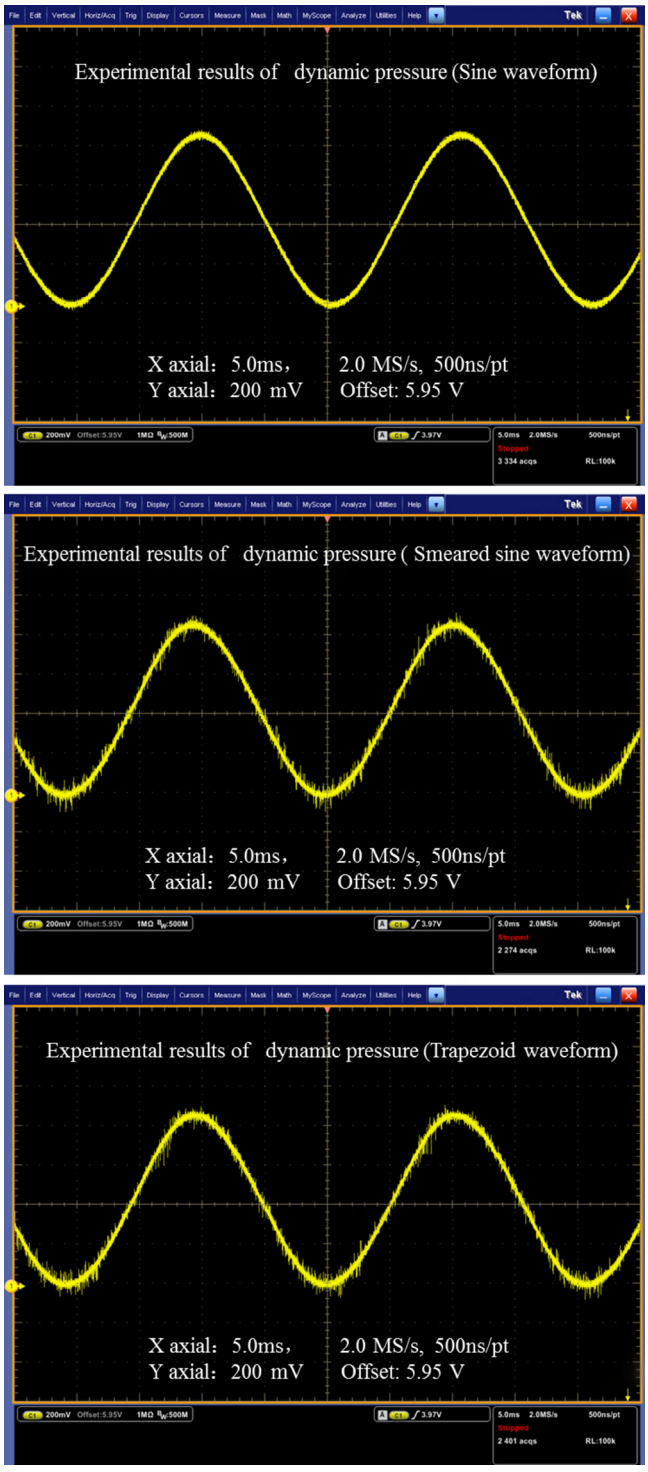

Fig. 9 – Experimental results of the dynamic pressure waveform under the three types of driving voltage waveform.

voltage has a pronounced effect on the cooling capacity of the SPTC.

As discussed above, a SPTC consists of two main parts, namely, the linear compressor and the cold finger, each of which has its specific efficiency. For the linear compressor, the motor efficiency is usually used to evaluate the compressor

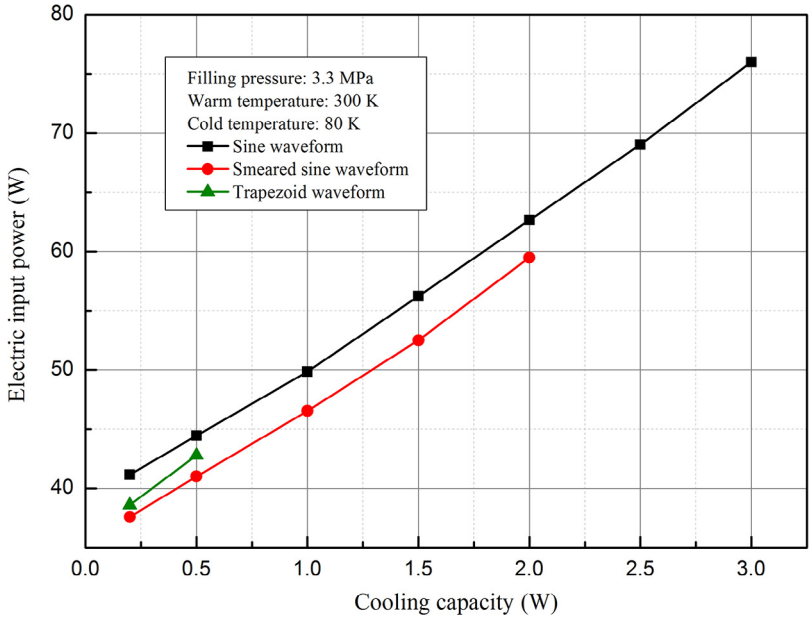

Fig. 10 – Relations between cooling capacity and electric input power under the three types of voltage waveforms.

performance. In the tests, both RMS current and RMS voltage are measured to calculate the coil losses and the motor efficiency. For each motor, the specific calculations of the motor losses and motor efficiency can be written as:

$$Q = I_{rms}^2 R_e \tag{4}$$

$$\eta_{motor} = \frac{W_e - I_{rms}^2 R_e}{W_e} \tag{5}$$

where Q is the Joule heat of the motor coil, R_e is the coil resistance, I_{rms} is the RMS current, W_e is the input electric power of each motor and η_{motor} is the motor efficiency.

Table 4 shows the power losses due to the Joule heating of the coil. When the input power is smaller than 30 W, the coil losses under the trapezoid waveform are slightly higher than those under the smeared sine waveform, and both of them are lower than those under the sine waveform. However, with the further increase of the input power, the difference in the coil losses under the smeared sine waveform and sine waveform becomes smaller.

In order to investigate the influence of the voltage waveform on the compressor performance in a detailed way, the motor efficiencies are illustrated in Fig. 11. It is observed that, under the sine waveform voltage, the motor efficiency has a relatively small variation and its average value is about 80%. While under both smeared sine and trapezoid waveforms, the motor efficiency decreases with the increasing input power, but both of them are higher than that of the sine waveform. The results about the motor efficiency are consistent with the analyses about the cooling capacity shown in Fig. 10. The following reasons have been found for the above experimental results. First, according to the relation between the current and the piston displacement shown in Eq. (2), the current is determined together by the second order, the first order and the zeroth order derivative terms of the piston displacement, but the values under the three types of waveforms vary somewhat, so the RMS voltage and current are different. Second, under the same input power, the RMS voltages under the smeared sine and trapezoid waveforms are very close, and either of them is high than that of the sine waveform. The largest RMS current is achieved by the sine waveform, which is followed by the trapezoid waveform and the smeared sine waveform in proper order.

In addition, it should be noted that, in Fig. 11, with the input power smaller than 30 W, the motor efficiencies under both the smeared sine and the trapezoid waveforms are higher than 90%, which is considerably excellent for the linear compressor used for the SPTCs which have a mean value of below 85%. The test results suggest a promising approach to achieve a linear compressor with a very high motor efficiency by the optimization of the voltage waveform.

In order to study the specific influence of the voltage waveform on the cooling performance of the cold finger, the lowest no-load temperatures with three types of waveform have been tested, as shown in Fig. 12. Generally, the cooling performance under the sine waveform is the best, and then followed by that under the trapezoid waveform and the smeared sine waveform in proper order. As analyzed above in Fig. 5, the waveform of driving voltage will affect the phase relation between the

Table 4 – Motor coil losses under different input powers and voltage waveforms.

Input power (W)	Motor coil losses (W)		
	Sine	Trapezoid	Smeared sine
10	2.44	0.35	0.30
20	3.81	1.09	0.83
30	5.64	2.31	1.84
40	7.94	6.49	4.35
50	10.25	–	7.29

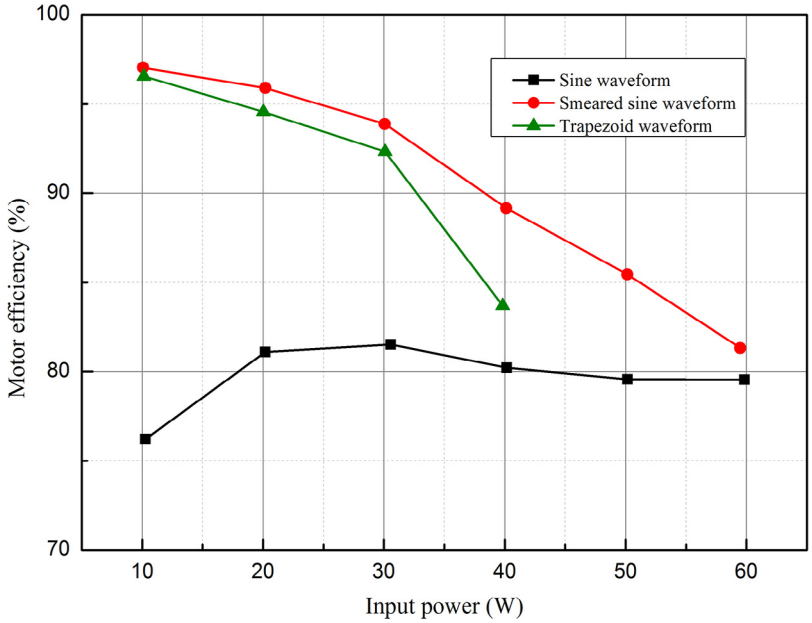

Fig. 11 – Variations of motor efficiency with input power under the three types of driving voltage waveforms.

dynamic pressure and the volume flow rate, but the developed cold finger is optimized based on the sine waveform, and thus the phase change caused by the voltage waveform will lead to the deterioration of the cooling performance of the cold finger.

Fig. 13 shows the relation between the electric input power and the lowest temperature under three types of waveforms. With the input power varying between 10 W and 20 W, the no-load temperature under the trapezoid waveform is the lowest, and the no-load temperature under the smeared sine waveform is lower than that of the sine waveform. With the input power varying between 30 W and 40 W, the no-load temperature under the trapezoid waveform becomes higher than that of the smeared sine waveform, but both of them are still lower than that of the sine waveform. Similarly, with relatively large input powers, the extra compressor vibration introduced by either trapezoid or smeared sine waveform will have an adverse effect on the cooling performance.

4. Discussions and conclusions

The operating parameters play a key role in understanding the working mechanisms of both the Stirling-type pulse tube cryocooler (SPTC) and its compressor, and also in enhancing their performance. However, the existing optimizations of these

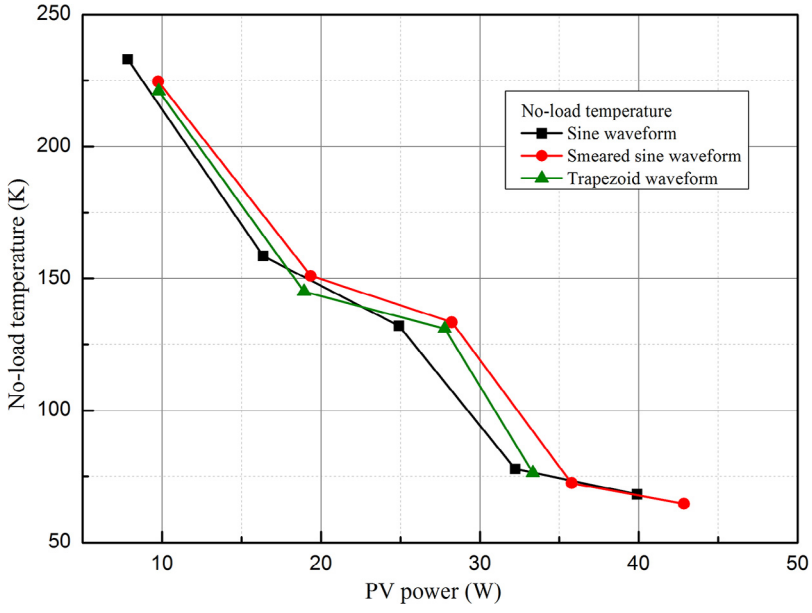

Fig. 12 – Relations between the lowest no-load temperature and the PV power under the three types of voltage waveforms.

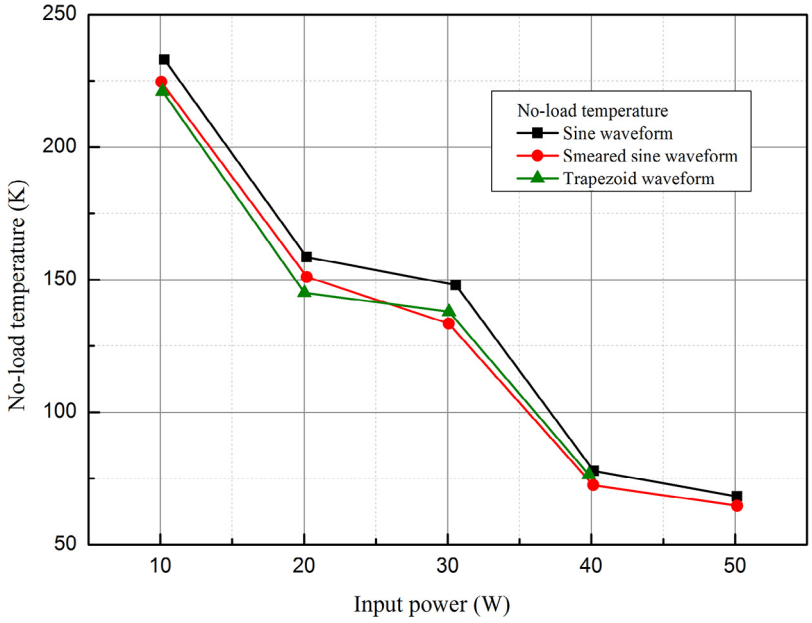

Fig. 13 – Relations between the lowest no-load temperature and the electric input power under the three types of voltage waveforms.

parameters mainly focus on the frequency, charge pressure, reject temperature, phase-shifting, and input voltage or current, etc., whereas the driving voltage waveform of the linear compressor is often overlooked.

In this paper, the effects of the drive voltage waveform on both the compressor motor efficiency and the cooling performance of the SPTC are studied. Two waveforms, namely, trapezoid and smeared sine are proposed, and then the corresponding performances under them are analyzed, tested and compared with that of the commonly-used sine waveform. The results indicate that the waveform plays an important role in affecting both the compressor motor efficiency and the cooling performance of the SPTC. In the tested range, both cooling efficiency and motor efficiency under either the smeared sine or the trapezoid waveform are higher than that of the sine one. Moreover, given that the input power is below 30 W, the motor efficiencies under both the smeared sine and the trapezoid waveforms exceed 90%, which suggests a promising approach to achieve a linear compressor with a very high motor efficiency by employing the optimized voltage waveforms.

It is also observed in the current experiments that, when the compressor input power is larger than 60 W, the extra compressor vibrations introduced by the discontinuity of the smeared sine waveform will become unacceptable, and thus in the present phase, this disadvantage limits their application range when compared with the commonly-used sine waveform to a great extent. At present, the focused is on addressing the problem and the relevant experiments are underway.

Acknowledgments

The work is financially supported by The National Basic Research Program of China (2013CB632802), The Aeronautical Science Foundation of China (20162490005) and The Science and Technology Commission of Shanghai Municipality (15521104900).

REFERENCES

Bailey, P.B., Dadd, M.W., Hill, N., Cheuk, C.F., Raab, J., Tward, E., 2001. High performance flight cryocooler compressor. In: Cryocoolers 11. Kluwer Academic/Plenum Press, New York, pp. 169–174.

Bailey, P.B., Dadd, M.W., Stone, C.R., 2010–2011. Cool and straight: Linear compressors for refrigeration. In: Proc. Inst. Refrigeration, 4-1.

Bradshaw, C.R., Groll, E.A., Garimella, S.V., 2011. A comprehensive model of a miniature-scale linear compressor for electronics cooling. Int. J. Refrigeration 34, 63–73.

Bradshaw, C.R., Groll, E.A., Garimella, S.V., 2013. Linear compressors for electronics cooling: energy recovery and its benefits. Int. J. Refrigeration 36, 2007–2013.

Dang, H.Z., 2012. 40 K single-stage coaxial pulse tube cryocoolers. Cryogenics 52, 216–220.

Dang, H.Z., 2015. Development of high performance moving-coil linear compressors for space stirling-type pulse tube cryocoolers. Cryogenics 68, 1–18.

Dang, H.Z., Zhang, L., Tan, J., 2016. Dynamic and thermodynamic characteristics of the moving-coil linear compressor for the pulse tube cryocooler. Part A: theoretical analyses and modeling. Int. J. Refrigeration 69, 480–496.

Davey, G., 1990. Review of the oxford cryocooler. Adv. Cryog. Eng. 35, 1423–1430.

Flaxer, E., 2003. Implementing of a precision fast thermoelectric cooler controller using a personal computer parallel port connection and ADN8830 controller. Rev. Sci. Instrum. 74, 3862–3873.

Gifford, W.E., Longsworth, R.G., 1965. Pulse tube refrigeration progress. Adv. Cryog. Eng. 10, 69–73.

Ki, T., Jeong, S., 2012. Step-by-step design methodology for efficient stirling-type pulse tube refrigerator. Int. J. Refrigeration 35, 1166–1175.
Kim, H., Roh, C., Kim, J., Shin, J., Hwang, Y., Lee, J., 2009. An experimental and numerical study on dynamic characteristic of linear compressor in refrigeration system. Int. J. Refrigeration 32, 1536–1543.
Kittel, P., Kashani, A., Lee, J.M., Roach, P.R., 1996. General pulse tube theory. Cryogenics 36, 849–857.
Liang, K., Stone, R., Dadd, M., Bailey, P., 2014. A novel linear electromagnetic-drive oil-free refrigeration compressor using R134a. Int. J. Refrigeration 40, 450–459.
Marquardt, E., Radebaugh, R., Kittel, P., 1993. Design equations and scaling laws for linear compressors with flexure springs. Cryocoolers 7, 783–804.
Ross, R.G., Jr., 2007. Aerospace coolers: a 50-year quest for long life cryogenic cooling in space. In: Timmerhaus, K.D., Reed, R.P. (Eds.), Cryogenic Engineering: Fifty Years of Progress. Springer, New York, pp. 225–284.
Walker, G., Bingham, E., 1994. Low-Capacity Cryogenics Refrigeration. Clarendon Press, Oxford.
Willems, D., Benschop, T., Groep, W., Mullié, J., Weijden, H., Tops, M., 2009. Update on Thales flexure bearing coolers and drive electronics, In: Proc. SPIE 7298.